Using the Near-Field Coupling of a Sharp Tip to Tune Fluorescence-Emission Fluctuations during Quantum-Dot Blinking

Eyal Shafran, Benjamin D. Mangum,* and Jordan M. Gerton†

Department of Physics and Astronomy, University of Utah, 115 South 1400 East, Salt Lake City, Utah 84112, USA

(Received 8 January 2011; published 13 July 2011)

We demonstrate that the cycling between internal states of quantum dots during fluorescence blinking can be used to tune the near-field coupling with a sharp tip. In particular, the fluorescence emission from states with high quantum yield is quenched due to energy transfer, while that from low-yield states is elevated due to field enhancement. Thus, as a quantum dot blinks, its emission fluctuations are progressively suppressed upon approach of a tip.

DOI: 10.1103/PhysRevLett.107.037403 PACS numbers: 78.67.Hc, 07.79.Fc, 68.37.Uv, 78.55.−m

The near-field interaction between a dipole emitter and a nanoscale structure is an intriguing problem that is important for a number of applications, including tip-enhanced microscopy and surface-enhanced spectroscopy. The field enhancement generated near sharp edges and tips via the electrostatic lightning-rod effect [1–5] and/or surface plasmon resonances [6–9], leads to an increase in an emitter's photoexcitation rate for separation distances below ~10 nm. On the other hand, the nanostructure can also reduce the fluorescence signal by providing external nonradiative relaxation channels to which the emitter can couple directly [10–13], by modifying the local density of optical states as in the Purcell effect [14], or by altering the radiation pattern of the emitter [15]. The net optical signal can thus be quite convoluted and difficult to interpret, except when one effect is dominant, or when the field enhancement can be reliably calculated, as is the case for metal nanospheres [11–13]; deconvolution can be difficult for nanostructures with arbitrary geometry.

The intrinsic quantum yield (q_0) of an emitter plays a central role in moderating its interaction with the environment. In particular, when q_0 is large, internal nonradiative relaxation processes are slow relative to radiative emission, so even weak quenching will noticeably decrease the fluorescence signal. On the other hand, when q_0 is small, internal relaxation is fast, making the fluorophore relatively insensitive to quenching and thus more sensitive to field enhancement. Some experiments have shown that larger signal enhancement factors are obtained for lower values of q_0 [2,16]. Here we demonstrate how different q_0 values, corresponding to different internal relaxation rates of an emitter, can be used to modify its interaction with a sharp tip by tuning the balance between quenching and enhancement. Large variations in the net fluorescence signal are observed, including a clear contrast reversal for gold tips. A simple analytical model is used to deconvolute the enhancement and quenching portions of the signal, revealing that gold tips exhibit both strong quenching and enhancement, while silicon tips exhibit nearly as strong enhancement but very weak quenching [1–5], and carbon nanotube (CNT) tips exhibit very strong quenching and no enhancement [17]. Finally, our measurements demonstrate explicitly that fast energy transfer suppresses emission fluctuations associated with blinking from emitters near metal surfaces, in agreement with recent observations of quantum dots on metal surfaces [18], nanoparticle films [19], and ITO [20].

To investigate how q_0 affects near-field interactions, we utilize the well-known phenomenon of fluorescence intermittency (blinking) in single semiconductor nanocrystal quantum dots (QDs) [21], Fig. 1(b). Single-photon counting experiments have revealed a correlation between a decrease in emission intensity and a decrease in the fluorescence lifetime [22–25], leading to the conclusion that a single QD can have many different internal states [24]. These studies in combination with extinction coefficient measurements showing similar absorption cross sections for low and high emissive states [26] suggest that the emission fluctuations are due to variations in q_0 corresponding to a relatively large number (~ 10) of states. We leverage these dynamic fluctuations in individual QDs to tune the near-field interactions via the value of

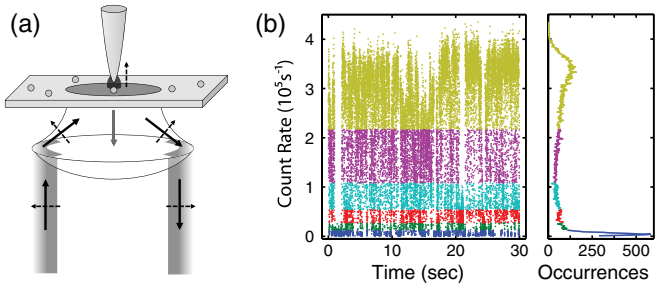

FIG. 1 (color online). Experimental scheme. (a) Excitation light is incident on the sample above the critical angle, creating an evanescent field above the sample with polarization along the axis of the tip. Fluorescence data are collected as the tip oscillates vertically above an isolated QD. (b) Photoluminescence trajectory from a single QD. The different colors illustrate the threshold levels in Figs. 2(a) and 2(b).

q_0. In particular, we use a novel photon counting technique [5] to capture interaction curves as a function of both q_0 and the spatial separation between a sharp atomic force microscope (AFM) tip and an individual QD.

When an AFM tip approaches the QD from above, the fluorescence signal will increase or decrease due to the various mechanisms described. Assuming the optical transition is not saturated, the far-field normalized fluorescence signal is then given by

$$S_{\mathrm{norm}}(z) = \frac{q(z)}{q_0}\kappa(z)\eta(z) = \frac{\Gamma_r + \Gamma_r'(z)}{\Gamma_0 + \Gamma'(z)}\frac{\kappa(z)\eta(z)}{q_0}, \quad (1)$$

where $q(z)$ is the effective quantum yield including modifications induced by the tip at height z above the QD, $\Gamma_0 = \Gamma_r + \Gamma_{\mathrm{nr}}$ is the intrinsic fluorescence rate including radiative (Γ_r) and nonradiative (Γ_{nr}) relaxation channels, and $\Gamma'(z) = \Gamma_r'(z) + \Gamma_{\mathrm{et}}(z)$ is the tip-induced relaxation rate. $\Gamma_r'(z)$ can be negative corresponding to a tip-induced suppression of the radiative rate and $\Gamma_{\mathrm{et}}(z)$ is the energy transfer rate from QD to tip. Finally, $\kappa(z) = I(z)/I_0$ is the far-field normalized excitation intensity at the QD, which includes tip-induced near-field effects, and $\eta(z) = C(z)/C_0$ is the ratio of the geometric collection efficiency in the presence, $C(z)$, and absence, C_0, of the tip. Equation (1) can be reparametrized as

$$S_{\mathrm{norm}}(z) = \frac{\alpha}{1 + q_0\beta}, \quad (2)$$

where $\alpha(z) \equiv \kappa(z)\eta(z)[1 + \Gamma_r'(z)/\Gamma_r]$ characterizes tip-induced changes to the local excitation intensity, the geometric collection efficiency, and the radiative rate, while $\beta(z) \equiv \Gamma'(z)/\Gamma_r$ characterizes the strength of the near-field coupling. The shape of a vertical approach-curve measurement, $S_{\mathrm{norm}}(z)$, for a particular value of q_0 reflects the dynamic balance between α and β. The values of α and β are extracted from measurements of S_{norm} for different values of q_0, as demonstrated below.

For light polarized along the z axis, the intensity at the tip apex should be enhanced due to the lightning-rod effect and/or surface plasmons. Furthermore, at short tip-sample distances z, the radiative rate of the fluorophore can be enhanced (i.e., $\Gamma_r' > 0$) due to the Purcell effect. These two mechanisms will increase α leading to signal enhancement. On the other hand, superposition of direct and tip-scattered excitation light at the QD can lead to a decrease in $\kappa(z)$ on a wavelength scale [5,12]. Furthermore, redirection of fluorescence emission toward the tip can modify η by no more than 50% for small tip-sample separations [10,27]. Nevertheless, α is typically dominated by near-field enhancement for $z < 50$ nm. The larger the product $q_0\beta$, the stronger the reduction in S_{norm}, so clearly a decrease in q_0 makes S_{norm} less sensitive to tip-sample coupling (quenching), and thus more sensitive to signal enhancement.

Data were obtained using a tip-enhanced fluorescence microscope (TEFM), which utilizes an AFM sitting atop a custom optical setup [5]. A continuous wave helium-neon laser ($\lambda = 543$ nm) is used as the excitation source. A small wedge of supercritical rays is allowed into the back aperture of a microscope objective (NA = 1.4) such that QDs are illuminated with a z-polarized evanescent field of intensity ~ 350 W/cm^2, Fig. 1(a). Using the measured extinction coefficient provided by the QD manufacturer (Invitrogen), the excitation rate is estimated to be a factor of 20 below saturation. The emitted photons are collected by the same objective and are focused onto an avalanche photodiode. The tip is aligned into the center of the focus spot and the sample is raster scanned. The AFM is operated in tapping mode with typical oscillation frequencies of 60–80 kHz and peak-to-peak amplitudes of 200–250 nm, depending on the specific probe. Several silicon, gold-coated, and homemade carbon nanotube (CNT) [28,29] AFM probes were used for the measurements described below. The sample consisted of elongated (4 nm × 9 nm) CdSe/ZnS QDs emitting at 605 nm, diluted in toluene and dried onto a glass coverslip. All data were taken at room temperature.

To extract vertical approach-curve measurements, $S_{\mathrm{norm}}(z)$, the lateral sample scan is halted when the tip is directly above a QD for the duration of a measurement (~ 30 s), and every detected fluorescence photon is then time stamped. Each signal photon is then correlated with the instantaneous height of the tip above the QD [1,5]. The photoluminescence trajectory from an individual QD is constructed using 1 ms time bins [Fig. 1(b)], and each photon is assigned a far-field count-rate value corresponding to its particular bin. Three important parameters are thus encoded with each signal photon: time of emission, tip height at the time of emission, and far-field count-rate value at that point in the fluorescence trajectory. The background signal is calibrated by moving the sample to an area with no QDs, and is subsequently subtracted carefully from the data. The count-rate uncertainty (1 kHz) associated with the 1 ms time bins is of minimal significance in the analysis: it is ~ 2 times smaller than the typical background rate and 3–5 times smaller than the average count rate within the lowest threshold range used to differentiate between states of different q_0.

Our data acquisition technique enables tip-sample approach curves to be reconstructed for different values of q_0. Figure 2 shows the unnormalized (a),(c) and normalized (b),(d) QD fluorescence signal as a function of the tip-sample distance for a gold-coated (a),(b) and silicon (c),(d) tip. For each tip, the various approach curves shown were extracted from a single 30-s measurement on a single QD: the photon data were first separated into several emission intensity thresholds, as illustrated in Fig. 1(b), and the z-dependent fluorescence signal was then reconstructed for each. The threshold ranges differ successively by a

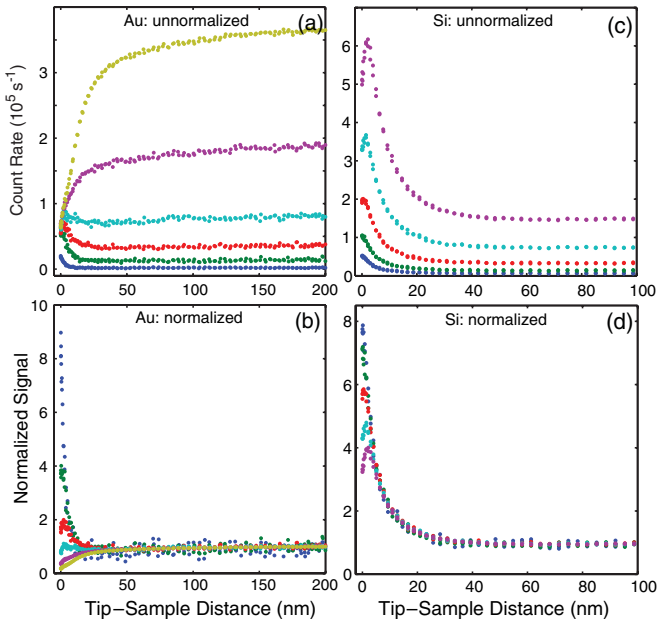

FIG. 2 (color online). Vertical approach curves for different count-rate thresholds. Un-normalized (a, c) and normalized (b, d) fluorescence signals as a function of the tip height above a QD for gold-coated (a, b) and silicon (c, d) probes. The color-coding in (a, b) corresponds to the threshold values shown in Fig. 1(b). For each tip, the various approach curves were obtained from a single measurement as the QD cycled dynamically through different quantum yield states.

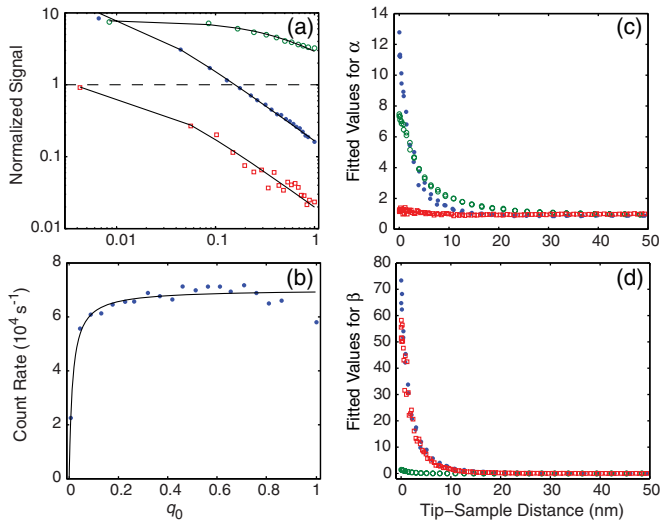

FIG. 3 (color online). Separation of enhancement and quenching. (a) Normalized signal at $z = 0$ and corresponding fit to Eq. (2) for gold-coated (blue solid circles), silicon (green open circles), and CNT (red open squares) tips. The dashed line separates enhancement and quenching. (b) Unnormalized fluorescence signal at $z = 0$ for the gold-coated tip in (a); the solid line is the best fit to Eq. (3). Panels (a) and (c) show the fitted values for α and β for different tip-sample distances.

factor of 2, which emphasizes the differences between the corresponding values of q_0.

For the gold-coated tip, Figs. 2(a) and 2(b), the bright states of the QD are strongly quenched as fast energy transfer to the tip outcompetes relatively slow intrinsic relaxation. In contrast, the darkest states are strongly enhanced as fast intrinsic relaxation outcompetes energy transfer, yielding more sensitivity to the enhanced field at the tip apex. The ratio of signal enhancement factors for the darkest state compared to the brightest one is $\sim 9/0.16 = 56$ at $z = 0$, as shown in Figs. 2(b) and 3(a) (note that a signal enhancement factor below unity indicates quenching). Thus, strong near-field coupling (large β) for gold tips amplifies changes in q_0 according to Eq. (2), leading to near-field contrast reversal for bright and dark states. Weak coupling between the silicon tip and QD imparts poor sensitivity to changes in q_0, as seen in Figs. 2(d) and 3(a). In this case, field enhancement is dominant for all values of q_0, although quenching does cause a minor decrease in signal at the smallest tip-sample separation distances. As q_0 becomes smaller, intrinsic relaxation of the QD outcompetes energy transfer at progressively smaller tip heights, until finally the signal increases monotonically as the tip approaches the QD.

Figure 3(a) plots S_{norm} at $z = 0$ as a function of q_0 for gold-coated, silicon, and CNT tips, where we have assumed that $q_0 = 1$ for the brightest state of a particular photoluminescence trajectory [23,30]. For these data, the highest far-field threshold corresponded to $\geq 70\%$ of the maximum count, in agreement with previous observations [23]. The remainder of each trajectory was divided linearly into as many distinct ranges as possible, so as to allow for sufficient signal-to-noise ratio in each. If the number of internal states is sufficiently large ($\gtrsim 10$), the system can be regarded as continuous and the results of the analysis will not be sensitive to the particular number of threshold ranges, N. This was verified by varying N between ~ 12 and 30 for each measurement. The data for each trajectory in Fig. 3(a) were fit to Eq. (2); the fits (solid lines) for all three tips are excellent across more than 100-fold variation in q_0. The dashed line separates signal enhancement and quenching: the near-field signal is dominated by enhancement for silicon tips, quenching for CNT tips, and can be tuned via q_0 to either enhancement or quenching for gold-coated tips.

The analysis was repeated at each value of tip-QD separation, and the fitting parameters α and β were extracted, as shown in Figs. 3(c) and 3(d). The maximum value for α is larger for gold-coated tips compared to silicon, reflecting stronger field enhancement at this wavelength (see [31] for polarization dependence of α and β). Without the aid of simulations or a geometry-dependent analytical model, it is not possible to determine this difference unambiguously with any other method, since gold-coated tips also quench the signal strongly: $\beta_{\text{Au}}/\beta_{\text{Si}} \sim 37$ at $z = 0$. The CNT tip induces no significant enhancement at any value of q_0 or z ($\alpha_{\text{CNT}} \sim 1$), but does quench the

signal strongly indicating efficient energy transfer between the QD and CNT at short separations [17].

Importantly, these measurements expose the mechanism responsible for the suppressed emission fluctuations associated with blinking from quantum emitters adsorbed onto conducting surfaces [18–20]. Figure 3(b) plots the unnormalized signal at $z = 0$ as a function of q_0, showing that the measured fluorescence rate is approximately constant down to $q_0 \sim 0.1$ (see [31] for similar plots at $z > 0$). Thus, in the case of a QD adsorbed onto a conducting surface ($z \sim 0$), the overall emission intensity is reduced due to quenching by the surface. As the QD blinks, it samples states with different q_0 values; however, the emission intensity is buffered by fast energy transfer from the QD to the surface. This is easily understood using our simple model: multiplying Eq. (2) by q_0 yields an expression that is proportional to the unnormalized fluorescence signal, $S(z)$:

$$S(z) \propto q_0 S_{\mathrm{norm}}(z) = \frac{q_0 \alpha}{1 + q_0 \beta}. \tag{3}$$

Thus, for large values of β, as for a gold-coated tip at $z = 0$, the product $q_0\beta \gg 1$ and until $q_0 \to 0$, the unnormalized signal will be independent of q_0: $S(z) \propto \alpha/\beta$. Importantly, the suppression of emission fluctuations is thus expected for any geometry or material for which β is large. The solid curve in Fig. 3(b) is the best fit line corresponding to Eq. (3), with $\alpha = 12.8$ and $\beta = 73.4$, as extracted from Figs. 3(c) and 3(d), and the proportionality factor as the only fitting parameter. When $q_0\beta \gg 1$, the fluorescence rate (relative to the far-field value) converges to α/β, which depends on the probe geometry and material. For gold-coated tips, $\alpha/\beta \sim 0.17$ at $z = 0$, so the fluorescence signal is nearly sixfold smaller than the maximum far-field value, and the suppression of emission fluctuations is discernible (see [31]). For CNT tips, $\alpha/\beta \sim 0.02$ so the fluorescence signal is suppressed by nearly a factor of 50, and it is difficult to detect the lack of fluctuations above the noise level.

In conclusion, the dynamic fluctuations in quantum yield that occur during QD blinking tune the balance between tip-induced enhancement and quenching, and make it possible to separate their contributions to the net fluorescence signal. Our measurements show that the near-field signal is dominated by enhancement for silicon tips, quenching for CNT tips, and can be tuned via q_0 to either enhancement or quenching for gold-coated tips. In addition, gold-coated tips strongly suppress the emission fluctuations associated with blinking, in agreement with previous observations of QDs adsorbed onto metal surfaces. Our measurements demonstrate explicitly that the lack of fluctuations is due to strong near-field coupling (large β) between the tip and emitter. In principle, the blinking fluctuations should also be suppressed if the radiative rate becomes large, $\Gamma_r' \gg \Gamma_r$, which might occur in an optical cavity, photonic crystal, or near a plasmonic nanoantenna.

This work was supported in part by the NSF and the Research Corporation for Science Advancement.

*Present address: Nanotechnology and Advanced Spectroscopy Team, Los Alamos National Laboratory, Los Alamos, New Mexico, USA.

†jgerton@physics.utah.edu

[1] J. M. Gerton *et al.*, Phys. Rev. Lett. **93**, 180801 (2004).
[2] V. Protasenko, A. Gallagher, and D. Nesbitt, Opt. Commun. **233**, 45 (2004).
[3] V. Protasenko and A. Gallagher, Nano Lett. **4**, 1329 (2004).
[4] E. Yoskovitz *et al.*, J. Phys. Chem. C **112**, 16306 (2008).
[5] B. D. Mangum *et al.*, Nano Lett. **9**, 3440 (2009).
[6] T. H. Taminiau *et al.*, Nat. Photon. **2**, 234 (2008).
[7] P. Muhlschlegel *et al.*, Science **308**, 1607 (2005).
[8] J. Farahani *et al.*, Phys. Rev. Lett. **95**, 017402 (2005).
[9] L. Novotny, Phys. Rev. Lett. **98**, 266802 (2007).
[10] N. A. Issa and R. Guckenberger, Opt. Express **15**, 12131 (2007).
[11] P. Anger, P. Bharadwaj, and L. Novotny, Phys. Rev. Lett. **96**, 113002 (2006).
[12] S. Kühn *et al.*, Phys. Rev. Lett. **97**, 017402 (2006).
[13] R. Carminati *et al.*, Opt. Commun. **261**, 368 (2006).
[14] E. M. Purcell, Phys. Rev. **69**, 681 (1946).
[15] H. Gersen *et al.*, Phys. Rev. Lett. **85**, 5312 (2000).
[16] H. G. Frey, J. Paskarbeit, and D. Anselmetti, Appl. Phys. Lett. **94**, 241116 (2009).
[17] E. Shafran, B. D. Mangum, and J. M. Gerton, Nano Lett. **10**, 4049 (2010).
[18] Y. Ito, K. Matsuda, and Y. Kanemitsu, Phys. Rev. B **75**, 033309 (2007).
[19] X. Ma *et al.*, Nano Lett. **10**, 4166 (2010).
[20] S. Jin, N. Song, and T. Lian, ACS Nano **4**, 1545 (2010).
[21] A. L. Efros and M. Rosen, Phys. Rev. Lett. **78**, 1110 (1997).
[22] G. Schlegel *et al.*, Phys. Rev. Lett. **88**, 137401 (2002).
[23] B. Fisher *et al.*, J. Phys. Chem. B **108**, 143 (2004).
[24] K. Zhang *et al.*, Nano Lett. **6**, 843 (2006).
[25] D. Montiel and H. Yang, J. Phys. Chem. A **112**, 9352 (2008).
[26] P. Kukura *et al.*, Nano Lett. **9**, 926 (2009).
[27] T. H. Taminiau, F. D. Stefani, and N. F. Van Hulst, New J. Phys. **10**, 105005 (2008).
[28] J. Hafner *et al.*, J. Phys. Chem. B **105**, 743 (2001).
[29] C. Mu *et al.*, IEEE J. Sel. Top. Quantum Electron. **14**, 206 (2008).
[30] X. Brokmann *et al.*, Phys. Rev. Lett. **93**, 107403 (2004).
[31] See Supplemental Material at http://link.aps.org/supplemental/10.1103/PhysRevLett.107.037403 for additional information.